

# Protein-Based Hydrogels that Actuate Self-Folding Systems

Conor M. Gomes, Chang Liu, Jeffrey A. Paten, Samuel M. Felton, and Leila F. Deravi\*

An approach to build a chemomechatronic system inspired by self-folding robots is described. This system, which comprises a protein-based hydrogel bound to a low-profile laminate, responds to different aqueous environments by undergoing geometric transformations. This response is dependent on the thickness and stiffness of the templating hydrogel, which directly regulates the diffusion of water into and out of the platform to initiate its reversible shape changes. When modified to include more complex geometries, these controllable shape changes can also be used to selectively trigger multiple folding events, illustrating a new platform for chemically initiated mechatronic devices. Together, these data show how compositionally discrete components are physically, chemically, and mechanically coupled together to generate a new actuator for biohybrid self-folding systems.

## 1. Introduction

Self-folding systems offer a robust platform for assembling complex, multicomponent devices across multiple spatial scales<sup>[1]</sup> ranging from macroscopic robots<sup>[2]</sup> to microscale surgical tools.<sup>[3]</sup> The components of a self-folding technology include a rigid substrate, a flexible region that serves as a hinge, and a material responsive to one or multiple forms of stimulation (current,<sup>[4]</sup> voltage,<sup>[5]</sup> temperature,<sup>[6]</sup> light,<sup>[7]</sup> pressure,<sup>[8]</sup> or pH<sup>[9]</sup>). Self-folding technologies also show great potential for generating reconfigurable biomaterial interfaces which can be useful in delivering cargo<sup>[3a,10]</sup> or navigating complex geometries<sup>[11]</sup> in the body; however, these applications introduce new design considerations such as the need for biocompatible materials and compact, long term power sources. A popular material used to overcome the barrier of biocompatibility is polydimethylsiloxane (PDMS), which achieves shape-based changes via pneumatic-based actuators<sup>[12]</sup> designed to mimic human functions such as muscle contraction.<sup>[13]</sup> Although PDMS is biocompatible, it relies on pneumatic actuation that translates poorly for long-term in vivo applications due to its dependence on an external power source. Thus, new materials are required

to overcome the dependency, especially as devices continue to miniaturize and increase in complexity.


Soft, biomimetic hydrogels are an attractive alternative for actuation that have facile fabrication techniques with increased biocompatibility.<sup>[14]</sup> Hydrogels can absorb  $\approx 90\%$  of their mass in water, resulting in significant changes to its 3D architecture<sup>[15]</sup> that can be tuned to respond to a wide range of external stimuli including changes in pH,<sup>[16]</sup> temperature,<sup>[17]</sup> and analyte concentration.<sup>[18]</sup> Hydrogel mechanics can also be modulated via cross-linking,<sup>[19]</sup> interpenetrating networks,<sup>[20]</sup> and/or nanoparticle integration,<sup>[21]</sup> to reduce actuation times ( $<1$  s)<sup>[22]</sup>

while increasing the complexity of achievable shapes upon hydration/dehydration.<sup>[23]</sup> In this paper, we evaluated a protein-based hydrogel as the active component in a self-folding composite. We designed a new biohybrid system that incorporated a bilayer material comprising aluminum chemically coupled to the hydrogel. Gelatin was used as a model protein for our system because of its robustness, low cost, and ability to spontaneously form a hydrogel in ambient conditions.<sup>[24]</sup> We investigated how changes in hydrogel mechanics, thickness, and cross-linking density influenced the kinetics of folding (i.e., actuation) under different aqueous environments.

Actuation was achieved through dehydrating the biohybrid system in polyethylene glycol (PEG) and reversed via hydration in sodium chloride (NaCl). PEG, a commonly used biodegradable and biocompatible polymer,<sup>[25]</sup> also exhibits deliquescence, a feature that can offer precise control over the steady-state dehydration of the hydrogel to effectively eliminate effects associated with humidity-induced variability.<sup>[26]</sup> While the use of PEG has been successfully implemented for applications ranging from concentrating collagen molecules in solution,<sup>[27]</sup> driving optical clearing in skin tissue,<sup>[28]</sup> and regulating collagen fibril diameter and spacing in the cornea,<sup>[29]</sup> it has yet to be used to stimulate hydrogel actuation. Thus, we explored whether these properties could be leveraged to selectively remove the water from within a hydrogel without compromising the network. We monitored dimensional changes exhibited by the hydrogels during actuation using bright-field microscopy and analyzed the kinetic behavior of these changes using a modified lumped-capacitance model.<sup>[30]</sup> From this model, we quantified the time constants associated with folding and unfolding, as well as identified how the presence of water influenced folding velocity. Our data indicate the utility of biohybrid actuators that control self-folding within aqueous environments supported with new methods to relate the hydration state of the bound hydrogel to the degree of actuation.

C. M. Gomes, Dr. J. A. Paten, Prof. L. F. Deravi  
Department of Chemistry and Chemical Biology  
Northeastern University  
Boston, MA 02115, USA  
E-mail: l.deravi@northeastern.edu

C. Liu, Prof. S. M. Felton  
Department of Mechanical and Industrial Engineering  
Northeastern University  
Boston, MA 02115, USA

 The ORCID identification number(s) for the author(s) of this article can be found under <https://doi.org/10.1002/adfm.201805777>.

DOI: 10.1002/adfm.201805777

## 2. Results and Discussion

### 2.1. Characterization of the Effect of Initial Gelatin Thickness on Actuation

In building a protein-based actuator, we first coated a laminated trilayer system comprising two rigid aluminum layers (thickness of each = 100  $\mu\text{m}$ ) and a flexural nylon layer (25  $\mu\text{m}$  thick) with polydopamine (PDA) (Figure 1). Next, a gelatin-based hydrogel cross-linked with a 4% wt/v microbial transglutaminase (mTG) solution was deposited onto the system creating the biohybrid material. In our platform, PDA was used as a chemical anchor to specifically couple the amine-containing residues of gelatin with the metal substrate similar to previous reports,<sup>[31]</sup> and mTG was used to enzymatically cross-link gelatin monomers to form the thermostable hydrogel network on the PDA-coated aluminum surface.<sup>[32]</sup> To test whether this system folded in an aqueous environment, water was selectively removed from the hydrogel using a 25% wt/v PEG solution. This solvent-induced actuation (e.g., folding) occurred over several hours. To rehydrate the hydrogel and unfold the system, the PEG solution was substituted for a 0.1 mol L<sup>-1</sup> NaCl solution, and the hydrogel expanded to elongate the structure

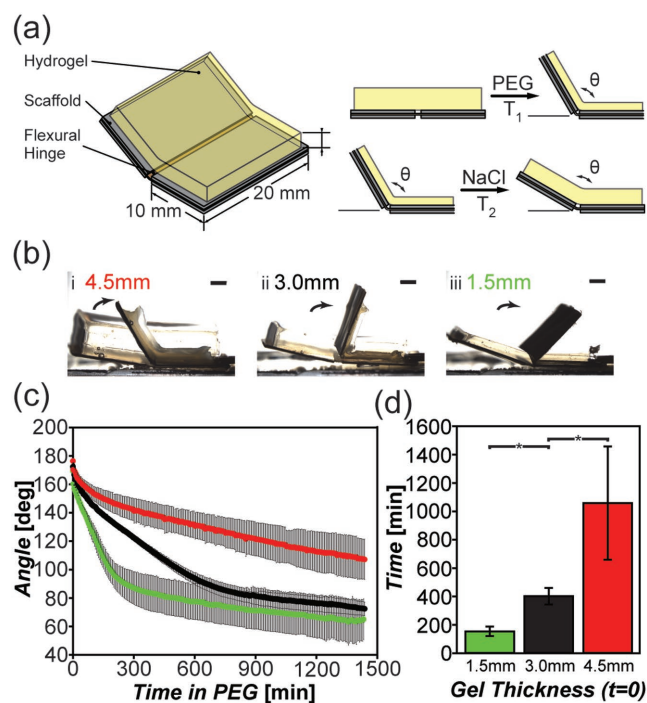


**Figure 1.** a) Representative schematic of the gelatin–aluminum–nylon system along with their predicted responses when introduced to a dehydrating (PEG) or hydrating (NaCl) aqueous environment. b) Images of the initial hydrated positions overlaid with the positions after 24 h in PEG solution (e.g., folded/dehydrated state) with a starting hydrogel thickness of i) 4.5, ii) 3.0, and iii) 1.5 mm (scale bar = 2.0 mm). c) The time-dependent internal angle measurements in PEG solution and the d) time each system takes to actuate 60° in a PEG solution with starting hydrogel thicknesses of 4.5 (red), 3.0 (black), and 1.5 mm (green) ( $n = 3$ ; error bars indicate standard deviation). d) Time in which the internal angle of the 1.5 (green), 3.0 (black), 4.5 mm (red) hydrogel actuated 50% of the total folding angle ( $n = 3$ ; error bars indicate standard deviation).

(Figure 1a). This process was reversible over multiple cycles (Figure S1, Supporting Information), illustrating its robustness in the different exchangeable solvent conditions.

Folding of the system in these different environments was tracked optically (Figure 1b), and changes in the internal bending angle as a function of hydrogel thickness were observed over 24 h (Figure 1c). When the initial thickness of the hydrogel was doubled and tripled, there was a significant decrease in the speed of actuation and magnitude of bending. For instance, the 1.5 mm thick hydrogels reached  $\approx 50\%$  of their total bending magnitude at  $154 \pm 33$  min (final angle achieved at 1444 min,  $65^\circ \pm 14^\circ$ ) compared to the 3.0 mm hydrogels at  $403 \pm 58$  min (final angle achieved at 1444 min,  $72^\circ \pm 5^\circ$ ), and 4.5 mm hydrogels at  $1058 \pm 400$  min (angle achieved at 1444 min,  $107^\circ \pm 14^\circ$  Figure 1d). These data suggest that the actuation speed and angle of the system were tunable by varying the initial thickness of the hydrogel.

### 2.2. Characterization of the Effect of Cross-Linking on Actuation

Because covalent cross-links are known to enhance the structural integrity of gelatin,<sup>[23,24b]</sup> the hydrogel thickness was fixed at 3.0 mm to isolate the effects of increasing cross-linking on actuation behavior, where we assumed that amount of cross-linking agent added to our system correlated with an increase in cross-linking density of the hydrogel network, similar to previous reports.<sup>[33]</sup> We found that increasing the cross-linking density of mTG from 0% to 4% elongated the actuation profile to yield a slower rate of folding (Figure 2a). When rehydrating, all systems expanded by  $\approx 90\%$  at 200 min (Figure 2b); however, the addition of the covalent cross-links decreased the magnitude of recovery, with 0% mTG recovering to  $179^\circ \pm 1^\circ$ , while 1% and 4% mTG only recovered to  $153^\circ \pm 6^\circ$  and  $145^\circ \pm 12^\circ$ , respectively (Figure 2b). Comparing the final angles achieved in all systems, cross-linking did not have a significant effect on

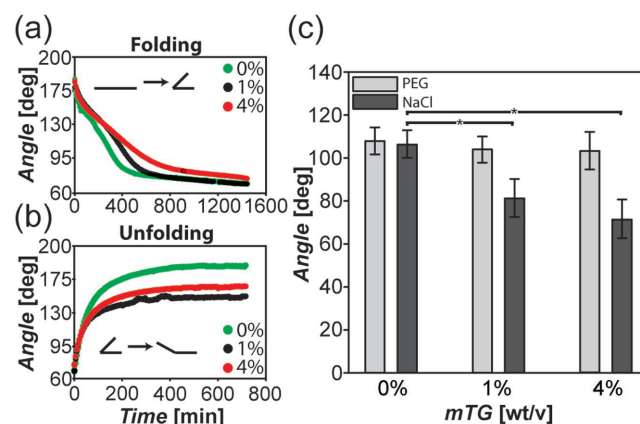


**Figure 2.** a) Representative trials ( $n = 1$ ) of time-dependent internal angle measurements of 3.0 mm gels while in PEG solution with 4% (red), 1% (black), and 0% (green) wt/v mTG. b) Representative trials ( $n = 1$ ) of time-dependent internal angle measurements while in NaCl solution with 4% (red), 1% (black), and 0% (green) wt/v mTG. c) The total amount of bending that occurred when the hydrogel system was placed into PEG then NaCl solution and actuates to completion ( $n = 3$ ; error bars indicate standard deviation).

the total magnitude of folding, but it did significantly reduce the ability to recover when rehydrated (Figure 2c). Despite these changes, varying the amount of covalent cross-linking did not correlate with the percent recovered, as the 1% and 4% hydrogels were not significantly different.

### 2.3. Model Fitting and Analysis

In the folding profiles reported in Figures 1c and 2a, we observed that the folding behavior of this biohybrid system was not a simple exponential decay. Instead, two inflection points were present, which indicated multiple kinetic steps within our system. To better characterize this behavior, the transition point between these steps was identified as the maximum convexity between the two concave regions of the curve (Figure S2, Supporting Information). From this analysis, we interpolated transition points by using a modified lumped-capacitance model,<sup>[30]</sup> represented as

$$\begin{cases} \theta(t) = \theta_{\infty_1} + a_1 e^{-\frac{t}{\tau_1}} & \text{if } t < t_1 \\ \theta(t) = \theta_{\infty_2} + a_2 e^{-\frac{t}{\tau_2}} & \text{if } t > t_1 \end{cases} \quad (1)$$

where  $\theta(t)$  is the internal angle (deg) at time  $t$  (min),  $t_1$  is the transition point (min),  $\theta_{\infty_1}$  and  $\theta_{\infty_2}$  are the plateau angles of the first and second fits (deg), and  $a_1$  and  $a_2$  are constants. The time constants,  $\tau_1$  and  $\tau_2$  (min), were extrapolated from each condition, where  $\tau_2$  was associated with the approach to the theoretical minimum. When increasing the initial thickness of the hydrogel, the transition point was significantly delayed, resulting in a 175% increase in time between the 1.5 and 4.5 mm thick hydrogels (Figure 3a). Because the

lumped-capacitance model is thickness dependent,<sup>[30a]</sup> the time constants could not be compared across all thicknesses directly. However, we did note that  $\tau_1$  was always smaller than  $\tau_2$  across all conditions (Figure 3b), suggesting a “fast” and “slow” phase of contraction during dehydration in PEG.

When thickness was fixed at 3.0 mm and cross-linking was increased, we also observed an increase in the time to reach the transition points (Figure 3c). Time constants for the 0%, 1%, and 4% cross-linked samples were similar ( $\tau_1 = 139 \pm 51$ ,  $166 \pm 82$ , and  $186 \pm 12$  min for 0%, 1%, and 4%, respectively;  $\tau_2 = 193 \pm 16$  and  $195 \pm 11$  min for 0% and 1%, respectively), with only  $\tau_2$  of 4% ( $321 \pm 32$  min) being significantly different from the 0% and 1% cross-linked samples (Figure 3d). The final bending angles of all conditions were similar, averaging  $70^\circ \pm 13^\circ$  (Figure 2a), suggesting that the increase in covalent cross-linking only affected the time it took to achieve the minimum angle during actuation.

Rehydrating the systems occurred much faster than the dehydrating processes and did not exhibit a transition point (Figure 2b), thus was fit to a single function

$$\theta(t) = \theta_0 + a \left( 1 - e^{-\frac{t}{\tau}} \right) \quad (2)$$

where  $\theta_0$  is the angle (deg) at  $t = 0$ , with  $\tau$  values significantly lower than those derived from the contraction. Rehydration  $\tau$  values were similar (e.g.,  $93 \pm 11$  and  $91 \pm 8$  min, for 0% and 4% mTG, respectively, Figure 3d), indicating that while the magnitude of recovery differed, the time to recover was the same regardless of cross-linking density.

### 2.4. Characterizing Gel Thickness Changes During Actuation

To better understand why cross-linking affected the kinetics but not the total magnitude of folding, we investigated the dimensional change that the hydrogels exhibited during dehydration in PEG. We hypothesized that the kinetic behavior of contraction was regulated by water diffusion through the hydrogel, where  $\tau_1$  was associated with water that could easily be liberated (referred to as polymolecular water), and  $\tau_2$  was associated with tightly integrated water (referred to as structural and monomolecular water) within the hydrogel, similar to previous reports.<sup>[34]</sup> To test this hypothesis in our system, we monitored the change in hydrogel thickness as a function of cross-linking density, which is a known parameter that regulates water diffusion.<sup>[35]</sup> Starting with an initial thickness of 3.0 mm, we manually tracked the profile of the contracting hydrogels in PEG over time (Figure 4a) and observed no significant differences in the thicknesses that each system achieved using the different cross-linking densities (Figure 4b, inset). Each hydrogel ultimately plateaued to a final thickness averaging  $1.0 \pm 0.3$  mm. In our analysis, we also observed no transition point during the contraction; instead, each parameter followed a single decay function with  $\tau$  values of  $111 \pm 13$ ,  $131 \pm 9$ , and  $165 \pm 13$  min (Figure 4b).

When comparing the relationship between the angles achieved during contraction (plotted in Figure 2) with the hydrogel thicknesses reported in Figure 4, the variations in

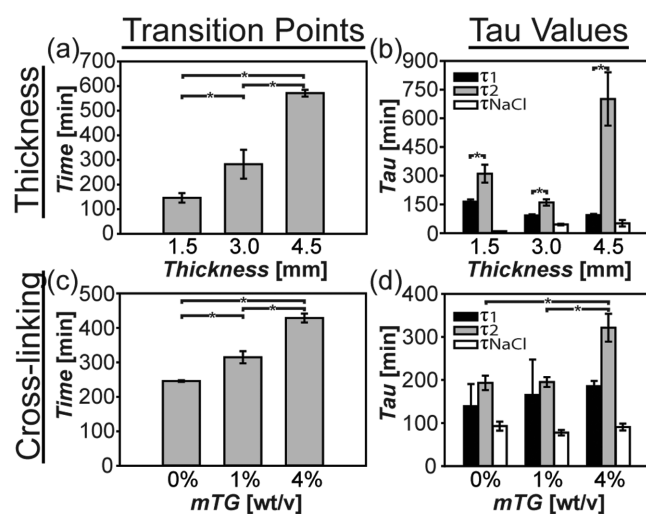


**Figure 3.** a) Calculated transition points when dehydrating each hydrogel (cross-linked with 4% w/v mTG) with initial starting thickness of 1.5, 3.0, and 4.5 mm. b) Calculated time constants when dehydrating each hydrogel with initial starting thickness of 1.5, 3.0, and 4.5 mm. c) Calculated transition points when dehydrating each hydrogel with mTG concentrations of 0%, 1%, and 4% wt/v. d) Calculated time constants when dehydrating each hydrogel with mTG concentrations of 0%, 1%, and 4% wt/v ( $n = 3$  for all samples; error bars indicate standard deviation).

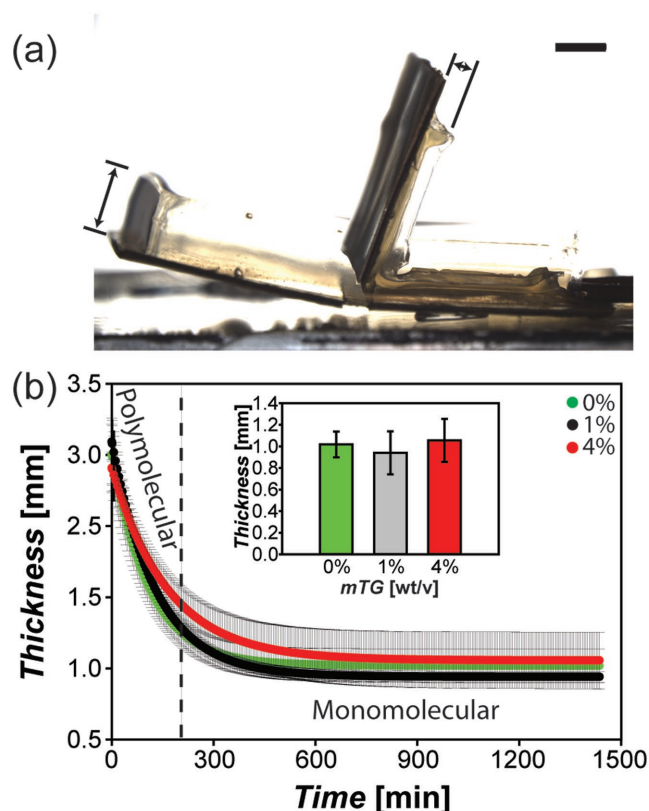


**Figure 4.** a) Optical images of the system before and after dehydration in PEG solution with a starting hydrogel thickness of 3.0 mm with 4% cross-linking (scale bar = 2.0 mm). b) Thickness of gelatin hydrogel with 0%, 1%, and 4% wt/v mTG was manually tracked over time during dehydration in the PEG solution. Dashed line indicates approximate time where 50% of bending has occurred in the 1% sample. Each side of the line represents the major contributor to the kinetics (polymolecular and monomolecular water). (inset) Calculated ending hydrogel thickness when dehydrating each hydrogel with mTG concentrations of 0%, 1%, and 4% wt/v to completion ( $n = 3$  in all samples; error is standard deviation).

thickness did not linearly correlate with the angle achieved. For instance, hydrogel thickness had reduced by  $89 \pm 2\%$  at the transition point (dashed line, Figure 4b) in the 1% cross-linked sample, yet only  $\approx 35\%$  of the total angle folding had occurred. Similar contraction proportions were found for the other samples, where the 0% mTG gel had contracted  $90 \pm 4\%$ , and 4% mTG had contracted  $92 \pm 1\%$  at the transition point. Thus, our findings suggested that the kinetic forces before and after the transition point may be dependent on different forms of water diffusion within and throughout the hydrogel during actuation. As stated by Kozlov and Burdygina in their 1983 report describing water diffusion through a gelatin hydrogel,  $\approx 10\%$  of the water within a gelatin hydrogel is comprised of monomolecular water, which is tightly bound in the network.<sup>[34]</sup> If we assume that all contraction of the gelatin hydrogel thickness is caused by water loss from the network, then we can similarly attribute the last 10% of the total contraction profile to the removal of tightly bound water, as Kozlov and Burdygina described. Indeed, we experimentally validate this assumption in Figure 4b, where we observed that the last 10% of contraction happens only after the transition point (dashed line, Figure 4b).

We also confirmed that this finding was not due to simple solvent diffusion kinetics; when the solution was stirred during actuation, we observed a similar actuating behavior (Figure S3, Supporting Information).

These observations were further supported using attenuated total reflectance-infrared (ATR-FTIR) spectroscopy, where we monitored changes in the types of water bound within the hydrogel cross-linked with 4% wt/v mTG (Figure S4, Supporting Information). When the gels were freshly made, we observed a broad peak in the  $3000\text{--}3600\text{ cm}^{-1}$  range that is typically attributed to an abundance of water within the hydrogel.<sup>[36]</sup> We also observed smaller peaks associated with gelatin structure and their intermolecular cross-links at 1635, 1560, 1243, and  $1455\text{ cm}^{-1}$ , indicative of amide I, amide II, amide III, and aldimine, respectively.<sup>[23a]</sup> After dehydration in PEG for 24 h, we observed an increased resolution of peaks ranging from  $3200\text{ to }3500\text{ cm}^{-1}$ , which was reminiscent of peak shifts that were previously identified in collagen-based films exposed to varying relative humidity values.<sup>[37]</sup> In the collagen films, these peaks were attributed to a combination of tightly bound water ( $\approx 3210\text{ cm}^{-1}$ ), an amide peak ( $3330\text{ cm}^{-1}$ ), and a free, or loosely bound, water peak ( $3440\text{ cm}^{-1}$ ). In the spectra of our dehydrated gelatin-based hydrogel (Figure S4, Supporting Information), we observed what appeared to be two shoulders at  $\approx 3400$  and  $\approx 3200\text{ cm}^{-1}$  on the sides of a peak centered at  $3300\text{ cm}^{-1}$ , which we attributed to the emergence of chemical shifts associated with the loosely bound and tightly bound water, respectively. Even though these changes in the water profile were observed after the dehydration/hydration cycles, the chemical signature of gelatin ( $1635, 1560, 1243,$  and  $1455\text{ cm}^{-1}$ ) persisted, albeit at variable intensities, suggesting that gelatin structure remained intact during these cycles (Figure S4, Supporting Information). We attributed the changes in intensity to a higher concentration of gelatin at the surface of the ATR crystal when dehydrated. When taken together, these data suggested an important role for water diffusion in regulating the actuation of these biohybrid platforms.

## 2.5. Selective Self-Folding

While our initial investigation focused on the actuation behavior of a simple, one-hinged system, we were interested in expanding the capabilities of the platform to a more complex scaffold; thus, we scaled the fabrication of our system to create an 8-hinged system (Figure 5a–j). The transverse arms of the initial planar surface were casted with 1% and 4% cross-linked gelatin, where our goal was to demonstrate that these components could be selectively folded at desired rates (Figure 5). Upon actuation, the system folded from a planar conformation to a cubic orientation over  $\approx 20$  h, where the 1% cross-linked arms folded  $1.44\times$  faster than the 4% cross-linked arms over time (Figure 5k). In general, we observed folding rates of these multihinged systems that were  $\approx 13\%$  slower than the single-hinged systems. We believe that this difference was due in part to doubling the total mass of the scaffold to accommodate a more complex geometry, as well as interference between adjacent hinges due to overlap between edge effects in their strain patterns. Finally, and perhaps most importantly, in this

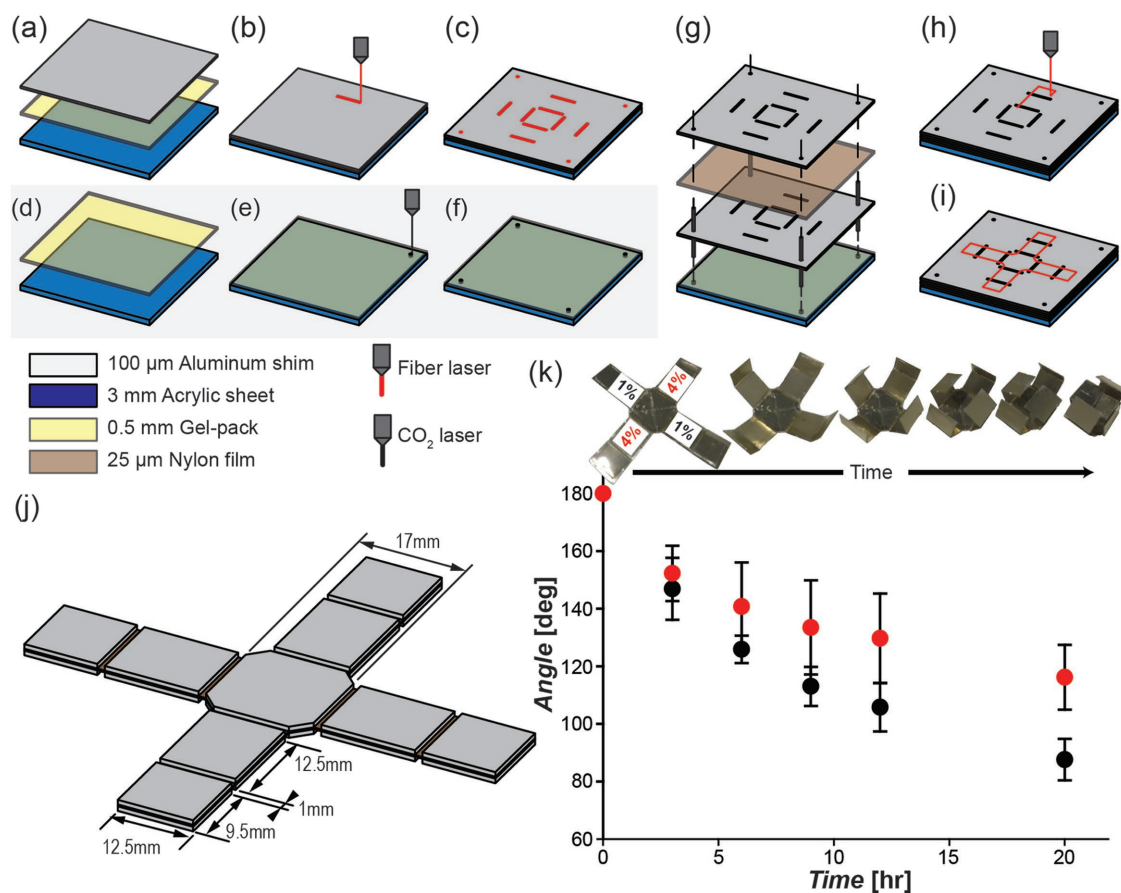


**Figure 5.** a) The layered assembly of a monolayer metallic scaffold, b) subsequent laser cutting of the adhered metal, c) final hinge cuts with hinge section and holes for pin alignment, d–f) pin alignment cut, g) pin alignment of multilayered scaffold, h,i) laser cutting of final cross design, j) final cross design, k) representative images of each time point in the graph with the average hinge angle angles for each cross-linker concentration.

demonstration the planar scaffold is folding against gravity; whereas, in the experiments preceding this (Figures 1–4), the single-hinged scaffold was fixed perpendicular to gravity, effectively reducing the effects associated with the scaffold weight from the system. Regardless of these challenges, we were able to illustrate a complex self-folding network templated by the gelatin-based hydrogel composite.

### 3. Conclusion

In this paper, we showed how chemically and mechanically coupling a protein-based hydrogel to a metal scaffold could facilitate self-folding under aqueous conditions. Distinguished from previous reports, our platform can be actuated by selectively removing and reinserting water complexed within a hydrogel during all phases of folding. Even though multiple kinetic events occurred as the scaffold folded during dehydration, a relatively fast unfolding occurred during rehydration, suggesting that the diffusion of water into and out of the scaffold directly regulates its dimensional changes. Furthermore, the ability to selectively control the rate of folding through modulating the cross-linking density permits the design of devices with greater geometric complexity, more sophisticated functionality (e.g., cyclable folding), and embedded electronic

features (as demonstrated by Liu et al.<sup>[38]</sup>)—all are important when considering the design of future implantable devices built to interface with and/or provide mechanical or electrical feedback to cells, tissues, and organs in the body during development, maturation, or regeneration. While our study was specific to gelatin-based hydrogel systems, we believe this platform technology can be translated to any natural or synthetic biopolymer system that is capable of grafting to or from a hinged scaffold while simultaneously and reversibly containing water within a 3D structure. When taken together, our findings offer fresh perspectives for designing new biohybrid, self-folding technologies that could conceivably be miniaturized as future implantable or assistive chemomechatronic devices.

### 4. Experimental Section

**Metallic Scaffold Assembly and Preparation:** The trilayer scaffold was designed with a flexural layer in between two rigid layers. The rigid layers were 100  $\mu\text{m}$  thick aluminum shim, and the flexural layer was 25  $\mu\text{m}$  nylon. GelPak (WF-60-X4-A) with adhesives on both sides was used to attach the aluminum shims to acrylic sheet to create flat cutting surface (Figure 5a). Aluminum shims were then cut using the fiber laser cutter (Universal Laser System, PLS6MW) with predesigned pattern (with holes for pin alignment and grooves for hinges) (Figure 5b,c). The cut aluminum shims were then cleaned by sonicating in 70% v/v ethanol

(Sigma) for 1 h and dried. A second set of acrylic with GelPak on top (Figure 5d) was cut using the CO<sub>2</sub> laser cutter (Figure 5e), with holes for pin alignment during assembly process (Figure 5f). Nylon film was sandwiched between two cleaned aluminum shims with adhesive, and the three layers were pin-aligned to adhere on the GelPak (Figure 5g). A release cut was used to cut out the outline (Figure 5h,i).

After final assembly, the scaffold was sonicated in 70% v/v ethanol and dried. After drying, the scaffold was placed in a 0.25% w/v Tris base (Sigma) for 10 min while stirring. Dopamine HCl (Sigma) was added while stirring to achieve a 0.2% wt/v solution. The scaffold was left in solution for 24 h, removed and sonicated in deionized water for 1 h, then dried under vacuum overnight. This process enabled PDA complexes to form with metallic atoms, as well as spontaneous bonds to form with amine-containing residues of gelatin,<sup>[31]</sup> ensuring covalent coupling of the protein hydrogel and the scaffold.

**Hydrogel Preparation:** Gelatin powder (Type A, 300 bloom, Electron Microscopy Sciences) was dissolved in deionized water at 60 °C to achieve 20% wt/v. T1 Transglutaminase Formula (Modernist Pantry) was dissolved in deionized water at 30 °C to achieve a desired % wt/v solution. The two solutions were mixed 1:1 before being applied to the PDA-coated metallic scaffold. The gel was cured for 1 h before any solvent was introduced to a PEG or NaCl solution, which is in agreement with previously published reports illustrating that 1 h is a sufficient curing time for the mTG cross-linked gelatin hydrogels.<sup>[39]</sup>

**Imaging and Data Production:** The scaffold was imaged using a Nikon SMZ18 stereoscope with an Imaging Source DFK 33UX174 camera. Images were captured using Nikon NIS Elements D Imaging Software. The scaffold demo was imaged using a GoPro Hero5 Session. Images were compiled and analyzed using ImageJ and MATLAB, respectively. Manual measurements of the gelatin hydrogel thickness were recorded using the imaging software ImageJ.

**Modeling and Statistical Analysis:** A lumped capacitance method<sup>[30]</sup> was used to model the folding behavior of the system. When dehydrating the gel in PEG, one or more exponential functions were fit to the data and the  $\tau$  values and the plateau values were compared. The lumped capacitance equation is shown in Equation (1). When hydrating in 0.1 M NaCl, the exponential function was fitted, shown in Equation (2).

Student's one-tail *t*-test was used to calculate a *p* value. If *p* < 0.05, the data were considered to be significantly different (notated by asterisk).

## Supporting Information

Supporting Information is available from the Wiley Online Library or from the author.

## Acknowledgements

The authors gratefully acknowledge the financial support from the Northeastern University Tier 1 Program and the National Science Foundation (Grant No. DMR-1700720, CMG LFD).

## Conflict of Interest

The authors declare no conflict of interest.

## Keywords

biohybrid, chemomechatronic, protein actuator, protein hydrogel, self-folding

Received: August 19, 2018  
Revised: October 12, 2018  
Published online:

- [1] a) M. E. W. Nisser, S. M. Felton, M. T. Tolley, M. Rubenstein, R. J. Wood, presented at 2016 IEEE/RSJ IROS, Daejeon, South Korea, October, 2016; b) S. H. Kang, M. D. Dickey, *MRS Bull.* **2016**, 41, 93.
- [2] a) C. Liu, S. M. Felton, presented at 2017 IEEE/RSJ Int. Conf. on Intelligent Robots and Systems (IROS), Vancouver, Canada, September, 2017, <https://doi.org/10.1109/IROS.2017.8206017>; b) S. Felton, M. Tolley, E. Demaine, D. Rus, R. Wood, *Science* **2014**, 345, 644.
- [3] a) A. Ghosh, C. Yoon, F. Ongaro, S. Scheggi, F. M. Selaru, S. Misra, D. H. Gracias, *Front. Mech. Eng.* **2017**, 3; b) C. Pacchierotti, F. Ongaro, F. van der Brink, C. Yoon, D. Prattichizzo, D. H. Gracias, S. Misra, *IEEE Trans. Autom. Sci. Eng.* **2018**, 15, 290.
- [4] A. Tselev, J. D. Budai, E. Strelcov, J. Z. Tischler, A. Kolmakov, S. V. Kalinin, *Nano Lett.* **2011**, 11, 3065.
- [5] J. Kaushik, T. J. Noah, D. Neel, G. Ben, J. W. Robert, *Smart Mater. Struct.* **2018**, 27, 065028.
- [6] A. Bhattacharyya, D. C. Lagoudas, Y. Wang, V. K. Kinra, *Smart Mater. Struct.* **1995**, 4, 252.
- [7] M. P. M. Dicker, A. B. Baker, R. J. Iredale, S. Naficy, I. P. Bond, C. F. J. Faul, J. M. Rossiter, G. M. Spinks, P. M. Weaver, *Sci. Rep.* **2017**, 7, 9197.
- [8] I. V. Uvarov, A. V. Postnikov, V. B. Svetovoy, *IOP Conf. Ser.: Mater. Sci. Eng.* **2016**, 108, 012032.
- [9] N. Bassik, B. T. Abebe, K. E. Lafin, D. H. Gracias, *Polymer* **2010**, 51, 6093.
- [10] a) W. Xu, K. S. Kwok, D. H. Gracias, *Acc. Chem. Res.* **2018**, 51, 436; b) J. C. Breger, C. Yoon, R. Xiao, H. R. Kwag, M. O. Wang, J. P. Fisher, T. D. Nguyen, D. H. Gracias, *ACS Appl. Mater. Interfaces* **2015**, 7, 3398.
- [11] a) S. Russo, T. Ranzani, J. Gafford, C. J. Walsh, R. J. Wood, presented at 2016 IEEE Int. Conf. on Robotics and Automation (ICRA), Stockholm, Sweden, May, 2016, <https://doi.org/10.1109/ICRA.2016.7487203>; b) J. H. Na, A. Evans Arthur, J. Bae, C. Chiappelli Maria, D. Santangelo Christian, J. Lang Robert, C. Hull Thomas, C. Hayward Ryan, *Adv. Mater.* **2015**, 27, 79.
- [12] a) Y. Hwang, R. N. Candler, *Lab Chip* **2017**, 17, 3948; b) O. Jeong, S. Konishi, *Sens. Actuators, A* **2007**, 135, 849.
- [13] A. Miriyev, K. Stack, H. Lipson, *Nat. Commun.* **2017**, 8, 596.
- [14] a) J. Stieghorst, T. Doll, *IEEE Trans. Biomed. Eng.* **2016**, 63, 2294; b) O. Ordeig, S. Y. Chin, S. Kim, P. V. Chitnis, S. K. Sia, *Sci. Rep.* **2016**, 6, 22803; c) E. Popa, V. Santo, M. Rodrigues, M. Gomes, *Polymers* **2016**, 8, 28.
- [15] E. M. Ahmed, *J. Adv. Res.* **2015**, 6, 105.
- [16] a) J. P. Best, M. P. Neubauer, S. Javed, H. H. Dam, A. Fery, F. Caruso, *Langmuir* **2013**, 29, 9814; b) H. Li, G. Go, S. Y. Ko, J.-O. Park, S. Park, *Smart Mater. Struct.* **2016**, 25, 027001; c) T. Traitel, J. Kost, presented at *Biomaterials*, Boston, MA, **2004**.
- [17] a) H. Warren, M. i. h. Panhuis, G. M. Spinks, D. L. Officer, *J. Polym. Sci., Part B: Polym. Phys.* **2018**, 56, 46; b) X. Zhang, C. L. Pint, M. H. Lee, B. E. Schubert, A. Jamshidi, K. Takei, H. Ko, A. Gillies, R. Bardhan, J. J. Urban, M. Wu, R. Fearing, A. Javey, *Nano Lett.* **2011**, 11, 3239.
- [18] a) Z. Mohammadi, S.-X. Xie, E. Peltier, M. Veisi, C. Berklund, *Eur. Polym. J.* **2011**, 47, 1485; b) H. F. El-Sharif, Q. T. Phan, S. M. Reddy, *Anal. Chim. Acta* **2014**, 809, 155.
- [19] a) V. Yesilyurt, M. Ayoob Andrew, A. Appel Eric, T. Borenstein Jeffrey, R. Langer, G. Anderson Daniel, *Adv. Mater.* **2017**, 29, 1605947; b) M. Pakulska Malgosia, K. Vulic, Y. Tam Roger, S. Shoichet Molly, *Adv. Mater.* **2015**, 27, 5002.
- [20] E. S. Dragan, *Chem. Eng. J.* **2014**, 243, 572.
- [21] a) M. Biondi, A. Borzacchiello, L. Mayol, L. Ambrosio, *Gels* **2015**, 1, 162; b) A. A. Hani, M. A. Hussain, A. Musab, N. Fozia Al, A.-H. Faten, O. Rahmi, K. Ali, *Biomed. Mater.* **2016**, 11, 014104.
- [22] a) G. Stoychev, L. Guiducci, S. Turcaud, W. C. Dunlop John, L. Ionov, *Adv. Funct. Mater.* **2016**, 26, 7733; b) E. Lee, D. Kim, H. Kim, J. Yoon, *Sci. Rep.* **2015**, 5, 15124.

- [23] a) J. Guan, H. He, D. J. Hansford, L. J. Lee, *J. Phys. Chem. B* **2005**, *109*, 23134; b) X. Peng, T. Liu, C. Jiao, Y. Wu, N. Chen, H. Wang, *J. Mater. Chem. B* **2017**, *5*, 7997.
- [24] a) A. Maddaus, P. Curley, M. A. Griswold, B. D. Costa, S. Hou, K. J. Jeong, E. Song, L. F. Deravi, *Biointerphases* **2016**, *11*, 041002; b) M. L. McCain, A. Agarwal, H. W. Nesmith, A. P. Nesmith, K. K. Parker, *Biomaterials* **2014**, *35*, 5462.
- [25] a) P. Jaipan, A. Nguyen, R. J. Narayan, *MRS Commun.* **2017**, *7*, 416; b) B. J. Klotz, D. Gawlitta, A. J. W. P. Rosenberg, J. Malda, F. P. W. Melchels, *Trends Biotechnol.* **2016**, *34*, 394.
- [26] a) J. A. Baird, R. Olayo-Valles, C. Rinaldi, L. S. Taylor, *J. Pharm. Sci.* **2010**, *99*, 154; b) J. Zhu, *Biomaterials* **2010**, *31*, 4639; c) J. Ulbricht, R. Jordan, R. Luxenhofer, *Biomaterials* **2014**, *35*, 4848; d) S. Gou, T. Yin, Q. Xia, Q. Guo, *RSC Adv.* **2015**, *5*, 32064.
- [27] J. A. Paten, G. E. Tilburey, E. A. Molloy, R. Zareian, C. V. Trainor, J. W. Ruberti, *Biomaterials* **2013**, *34*, 2577.
- [28] D. K. Tuchina, V. D. Genin, A. N. Bashkatov, E. A. Genina, V. V. Tuchin, *Opt. Spectrosc.* **2016**, *120*, 28.
- [29] S. Hayes, T. White, C. Boote, C. S. Kamma-Lorger, J. Bell, T. Sorenson, N. Terrill, O. Shebanova, K. M. Meek, *J. R. Soc., Interface* **2017**, *14*, 20170062.
- [30] a) F. P. Incropera, D. P. DeWitt, *Fundamentals of Heat and Mass Transfer*, Wiley, New York **1990**; b) C. R. Ruivo, J. J. Costa, A. R. Figueiredo, *Int. J. Therm. Sci.* **2008**, *47*, 282.
- [31] a) Y. Liu, H. Meng, S. Konst, R. Sarmiento, R. Rajachar, B. P. Lee, *ACS Appl. Mater. Interfaces* **2014**, *6*, 16982; b) J. Yang, V. Saggiomo, A. H. Velders, M. A. Cohen Stuart, M. Kamperman, *PLoS One* **2016**, *11*, e0166490; c) Z. Xu, *Sci. Rep.* **2013**, *3*, 2914.
- [32] G. Yang, Z. Xiao, H. Long, K. Ma, J. Zhang, X. Ren, J. Zhang, *Sci. Rep.* **2018**, *8*, 1616.
- [33] C. W. Yung, L. Q. Wu, J. A. Tullman, G. F. Payne, W. E. Bentley, T. A. Barbari, *J. Biomed. Mater. Res., Part A* **2007**, *83A*, 1039.
- [34] P. V. Kozlov, G. I. Burdygina, *Polymer* **1983**, *24*, 651.
- [35] Y. Wu, S. Joseph, N. R. Aluru, *J. Phys. Chem. B* **2009**, *113*, 3512.
- [36] K. S. Finnie, D. J. Cassidy, J. R. Bartlett, J. L. Woolfrey, *Langmuir* **2001**, *17*, 816.
- [37] S. Kudo, H. Ogawa, E. Yamakita, S. Watanabe, T. Suzuki, S. Nakashima, *Appl. Spectrosc.* **2017**, *71*, 1621.
- [38] C. Liu, C. M. Gomes, J. K. McDonald, L. F. Deravi, S. M. Felton, *Proc. SMASIS2018* **2018**, *2*, V002T02A005.
- [39] G. Yang, Z. Xiao, X. Ren, H. Long, H. Qian, K. Ma, Y. Guo, *PeerJ* **2016**, *4*, e2497.